Journal Pre-proofs

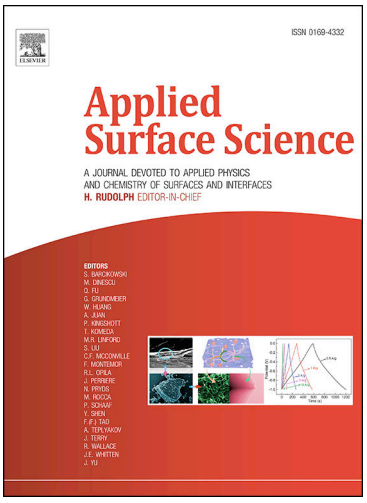

Full Length Article

Integration of phosphorylated MOF/COF core-shell structures into hybrid membrane for high-temperature fuel cell application

Kumar Divya, Qingqing Liu, Ravi Murali, Muhammad Rehman Asghar, Huiyuan Liu, Weiqi Zhang, Qian Xu, Jianwei Ren, Huaneng Su

PII: S0169-4332(24)02259-1
DOI: https://doi.org/10.1016/j.apsusc.2024.161544
Reference: APSUSC 161544

To appear in: *Applied Surface Science*

Received Date: 17 June 2024
Revised Date: 28 September 2024
Accepted Date: 15 October 2024

Please cite this article as: K. Divya, Q. Liu, R. Murali, M.R. Asghar, H. Liu, W. Zhang, Q. Xu, J. Ren, H. Su, Integration of phosphorylated MOF/COF core-shell structures into hybrid membrane for high-temperature fuel cell application, *Applied Surface Science* (2024), doi: https://doi.org/10.1016/j.apsusc.2024.161544

Integration of Phosphorylated MOF/COF Core-Shell Structures into Hybrid Membrane for High-Temperature Fuel Cell Application

Kumar Divya [a],Qingqing Liu [a], Ravi Murali [b], Muhammad Rehman Asghar [a],Huiyuan Liu [a], Weiqi Zhang [a], Qian Xu [a], Jianwei Ren [c], Huaneng Su [a,*]

[a] *Institute for Energy Research, Jiangsu University, 301 Xuefu Road, Zhenjiang 212013, PR China*

[b] *School of Materials Science and Engineering Jiangsu University, 301 Xuefu Road, Zhenjiang 212013, PR China*

[c] *Department of Chemical Engineering, University of Pretoria, cnr Lynnwood Road and Roper Street, Hatfield 0028, South Africa*

*Corresponding author

E-mail address: suhuaneng@ujs.edu.cn

Abstract

In the context of high-temperature proton exchange membrane fuel cells (HT-PEMFCs), the development of cost-effective and efficient proton exchange membranes (PEMs) is crucial. While PA-doped polybenzimidazole (PBI) membranes are commonly used in HT-PEMFCs, their synthesis involves complex processes and the use of carbogenic monomers. In this study, a novel hybrid PEM was synthesized by embedding individual UiO-67 MOF (microporous) , TABP@DMTP COF (mesoporous) and combined micro and mesoporous (MOF/COF) structures within sulfonated poly (ether ether ketone) (SPEEK) matrices. Phosphoric acid doping ensured anhydrous proton conductivity. The CM structures exhibited a core-shell arrangement with pore sizes of 1.7 and 3.2 nm, as confirmed by N_2 adsorption. Unlike MOF, COF and CM distribution within the SPEEK matrix enhanced PA doping levels. Specifically, the CM-embedded membrane showed the highest proton conductivity (7.6×10^{-3} S cm^{-1} at 130 °C) than commercial PA PBI (4.5×10^{-3} S cm^{-1} at 130 °C) under anhydrous conditions. Increasing CM content further enhanced membrane stability, as demonstrated by higher thermal degradation temperatures and tensile strength compared to PBI. Active functional

groups (SO_3H, NH) facilitated proton migration via acid-base interactions with phosphoric acid. Overall, the PASPCM-0.75 hybrid membrane achieved a balance between proton conductivity and mechanical stability, making it a promising candidate for anhydrous HT-PEMFC applications.

Key words: Poly (ether ether ketone), phosphoric acid, Core shell, Anhydrous proton conductivity, mechanical stability, high temperature fuel cell.

1. Introduction

Proton exchange membrane fuel cells (PEMFCs) are a promising clean energy technology for various sectors, including automotive, stationary power systems, and portable electronics [1, 2]. High-temperature PEMFCs (HT-PEMFCs) offer advantages over low-temperature PEMFCs due to enhanced carbon monoxide tolerance, electrode kinetics, water and heat management, and reduced need for cooling systems [3-6]. A key component of PEMFC longevity and efficiency is the proton exchange membrane (PEM), enabling proton transport while maintaining structural stability under extreme conditions [7, 8]. Using highly volatile acids to improve the performance of proton exchange membranes (PEMs) is a simple method to increase their operating temperature. The proton conductivity of PEMs doped with different acids varies [9, 10]. For instance, Xing et al.[11] observed the following order of proton conductivity in polybenzimidazole (PBI) membranes doped with different acids: HNO_3 > HCl > $HClO_4$ > H_2SO_4 > H_3PO_4. While H_2SO_4 exhibits the highest proton conductivity, achieving maximum conductivity in an H_2SO_4-based PBI membrane requires a minimum of 50% relative humidity (RH). Phosphoric acid is therefore considered a promising alternative in HT-PEMFC as it can operate effectively without the need for humidification or dependence on system humidity levels. The maximum proton conductivity of the PA-PBI polymer is attributed to the existence of free acids in the polymer structure and $H_2PO_4^-$/HPO_4^{2-} anionic chains, as described by Jones and Rozière [12]. The conductivity of the PA-PBI polymer is determined by the amount of phosphoric acid doped into it. However, excessive levels of phosphoric acid can limit the conductivity of pure PA-PBI by causing mechanical property degradation and acid leaching reduce the fuel performance [13, 14].

In recent years, considerable efforts have been directed towards developing alternative PEM materials using hybrid inorganic/organic crystal porous nanofillers. Especially metal organic framework such as University of Oslo [15], Zirconium series (UiO-66), Zeolite imidazole framework series (ZIF-8) [16], Material Institute Lavoisier (MIL-101) [17] and covalent organic framework hydrazone-linked COFs, includes a mixture of light elements (H, B, C, N, and O) held together by strong covalent bonds that crystallize into polymeric networks with highly ordered internal structures have emerged as promising candidates in HT-PEMFC [18]. The presence of designable porous nanostructures, large surface areas, and smaller band gaps of MOF and COF hybrids can significantly improve ion transport as well as molecular transfer and diffusion [19-21]. also enhances mechanical strength and thermal stability, thereby extending the operational range and durability of PEMFCs. Because of the complementary

effects of each of their constituent parts, MOF/COF heterostructures show many advantages for proton conduction when compared to individual MOFs or COFs. Further pi–pi conjugated structures in the plane and stacking direction, COFs exhibit increased chemical stability and conductivity, whereas pristine MOFs typically exhibit inadequate stability and limited conductivity. Consequently, there is an increase in stability and the potential to improve electrochemical properties like ion transfer ability when MOFs and COFs hybridize [22, 23].

The highest anhydrous proton conductivity of 1.4×10^{-2} S cm $^{-1}$ at 120 °C with an ultra-low activation energy is achieved by Liu et al. [19] synthesized imidazole molecules, which are encapsulated into core–shell UiO-67@TAPB–DMTP–COFs (TAPB = 1,3,5-tri (4-amino phenyl) benzene, DMTP = 2,5-dimethoxyterephthalaldehyde). Because of the rearrangement of hydrogen bonds and the improved transport of protons across the special heterogeneous channels, the synergism of porous MOF@COF heterostructures is very important for improving proton conduction. Similarly, Xu et al. [24] pioneered the loading of imidazole and pyrazole, respectively, into two-dimensional triphenylbenzene–2,5-dimethoxyterephthalaldehyde (TPB–DMTP) COFs, where the proton conductivity at 130 °C was found to be 4.37×10^{-3} S cm^{-1}. The high porous structure, active functional groups such as NH/NH_2 of COF allow the guest molecule inclusions and simplify the chemical modifications for example such Phosphoric acid anchored covalent organic frameworks have demonstrated high proton conductivity of 1.91×10^{-1} S cm^{-1} at 160 °C for TPB-DMTP-COF in an anhydrous environment. This exceptional conductivity is attributed to the unique characteristics of TPB-DMTP-COF, where the six N_{in} chains effectively anchor and strengthen the H_3PO_4 network within the channels. The strong N_{in}···H–O hydrogen-bonding interactions between the N_{in} chains and the H_3PO_4 network extend throughout the entire channel in a three-dimensional multichain multipoint mode. As a result, TPB-DMTP-COF not only stabilizes its pore structure but also reinforces the H_3PO_4 networks within the channels, creating a dually stable material [25].

Based on the attractive characteristics, mesoporous/microporous materials serve as a good proton source and are stable at elevated temperatures in HT-PEMFC. However, the core-shell MOF with polymer composite-based membrane has not been explored in HT-PEMFC. TAPB-DMTP-COFs, a typical Schiff base-type COF, was chosen as the shell material because of its exceptional stability and ultrahigh surface in a range of solvents. Through a Schiff-base condensation reaction, DMTP was used to interact with the amine group that UiO-67 provided in order to achieve the growth of the TAPB-DMTP-COFs shell on the surface of UiO-67 MOF. UiO-67 can be encapsulated into porous TAPB-DMTP-COFs to increase conductivity [26]. Therefore, in this work, we aim to design novel phosphoric acid doped SPEEK/UiO-67/TAPB–DMTP hybrid PEM and investigate the role of the core-shell MOF within the SPEEK membrane matrix. The incorporation of core-shell MOF is an emerging method in catalyst applications [27]. The individual properties of COF and MOF-based proton exchange membranes have been well studied in fuel cell applications, particularly for proton-conducting materials [28].

The combined properties of this heterogeneous porous structure incorporated into the PEM are less reported. Our study aims to investigate the role of individual MOF, COF, and combined MOF/COF core-shell properties within the sulfonated polymer. These polymers are economically favourable, offering the advantages of a simple synthetic route and being less expensive than commercial PBI. Furthermore, the hybrid composite containing core-shell structures provides a strong backbone for the membrane, enhancing chemical stability and increasing ionic mobility in the SPEEK matrix. The acid-base interaction between SPEEK,

core-shell MOF, and PA improves membrane performance in terms of anhydrous proton conductivity and thermal and mechanical stability and reduces PA loss, thereby extending the membrane operating temperature for HT-PEMFC applications. Performance evaluations with other PEMs, especially the PA-doped SPEEK/core-shell membranes, show excellent mechanical stability, overcoming the limitations of PA-doped PBI membranes. This research has the potential to significantly enhance the performance of HT-PEMFC applications, thereby contributing to the advancement of the field.

2 Material and methods

2.1 Chemicals

PEEK (Mw~35000) $[OC_6H_4OC_6H_4COC_6H_4]_n$, 1,4-dioxane, n-butanol, methanol, tetrahydrofuran, and N,N-dimethylformamide (DMF), 1-methyl-2-pyrrolidinone (NMP) Phosphoric acid, sulphuric acid was purchased from Mackiln Biochemical technology Co., Ltd. Shanghai. Anhydrous zirconium chloride supplied from INNOCHEM (Shanghai) ,1,3,5-tris (4-aminophenyl)-benzene(TAPB) and 2,5-dimethoxyterephthalaldehyde (DMTP), purchased from bidopharm, Shanghai. Biphenyl-4,4-dicarboxylic acid (BDA) and glacial acetic acid purchased MEYER, MREDA technology inc., Shanghai.

2.2 Fabrication of SPEEK

By using an electrophilic substitution reaction to post-sulfonate PEEK powder, SPEEK was synthesized. A solution of 5 g PEEK powder (98%) and 75 ml conc. H_2SO_4 (98%) was heated to 60 °C for 6 h approximately [29]. The detailed synthetic procedure reported in our previous paper and the prepared SPEEK characterized by ^1H Nuclear Magnetic Resonance (NMR) (Bruker Advanced III HD Nanobay 400 MHz FT-NMR spectrometer) polymer dissolved into DMSO d_6 Solvent.

2.3 UiO-67 MOF synthesis

UiO-67 is Synthesised via the hydrothermal method and the synthesis scheme given in Fig.1(a) [19]. Briefly, $ZrCl_4$ (0.2800 g, 1.2 mmol) and biphenyl-4,4-dicarboxylic acid (0.2906 g, 1.2 mmol) were dissolved into 30 mL DMF and 2 mL acetic acid at room temperature under constant stirring. The obtained white coloured mixture was transferred into a 100ml autoclave and heated at 120 °C for 48 h. Further, the product was washed with DMF for three times and allowed to dry in air and high temperature treatment at 300 °C for 24 h to remove the excess ligand and organic solvents. Finally, to obtain the pale yellow colored UiO-67 product.

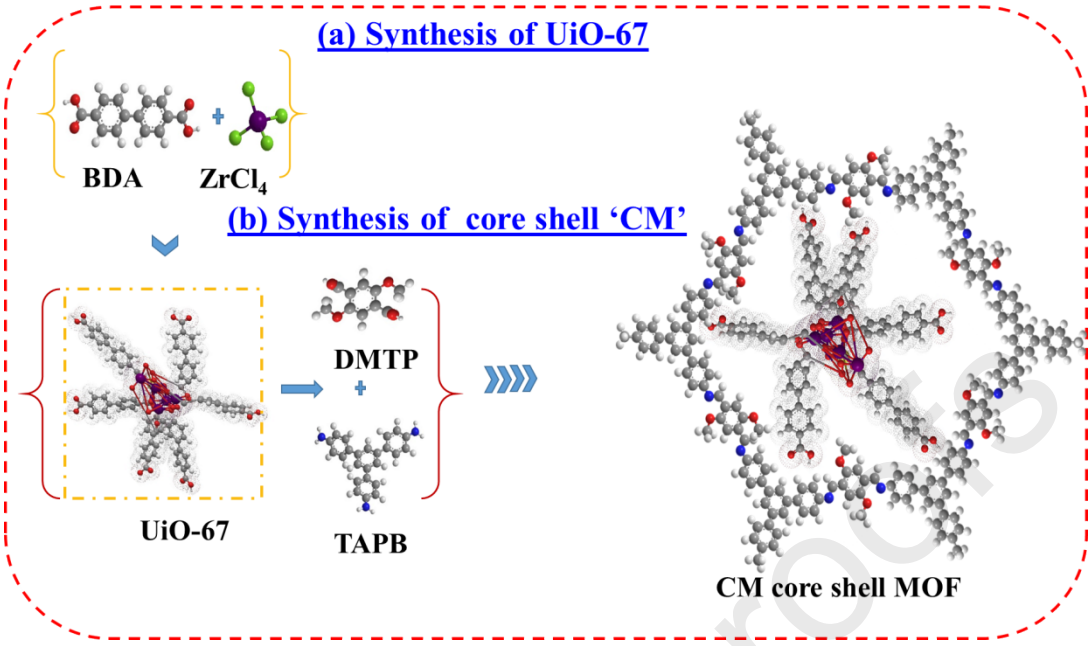

Fig.1(a) Schematic representation of UiO-67 (Hydrothermal method) and (b) UiO-67 MOF/ TAPB–DMTP-COFs (shiff base condensation reaction) core shell MOF synthetic root.

2.4 Synthesis of UiO-67 MOF/ TAPB–DMTP-COFs

The Core shell MOF synthesis scheme given in Fig.1(b). A mixture of 1,4-dioxane, n-butanol, and methanol (volume ratio 4:4:1) was used to dispersed 19 mg of UiO-67, 10.5 mg of TAPB, and 8.5 mg of DMTP in 4.5 mL. After 0.1 mL of acetic acid (3.0 mol L^{-1}) is added the above mixture, the reaction was allowed to run for 2 h at room temperature. Then 0.4 mL acetic acid was added and heated for 24 hours at 80 °C. Following the reaction, the precipitate was cleaned three times using tetrahydrofuran and vacuum-dried for 24 hours at 60 °C to produce a yellow powder known as 'CM'[19].Similarly, pristine TAPB/DMTP-COFs was synthesised via above method without addition of UiO-67 MOF.

2.5 Membrane Fabrication

SPEEK, SPEEK/UiO-67, SPEEK/COF and SPEEK/CM hybrid membranes are fabricated via simple solution casting method [30]. Additives such as UiO-67 $_X$, COF $_X$ and CM $_X$ (X=0.5 and 0.75%), dispersed into 90wt% NMP under ultra-sonication for a half hour.10wt% of SPEEK added into the above mixture with constant mechanical stirring for 6 h at room temperature to get a homogenous viscous solution (blend composition of polymer and filler wt.% and photocopy given in **Table S1 and Fig. S1**). After addition of filler content, the polymer dope solution colour changes were observed. Particularly pristine COF and CM fillers dramatically change the dope solution from pale yellow or dark yellow to red color. This is due to the acid-base reaction that occurs between SPEEK and CM/COF. Then, it was cast in a glass plate and dried in a vacuum oven at 80 °C for 24 h. Further, the resultant film was doped with 85% phosphoric acid solutions at 120 °C for 24 h and dried at 120 °C in a vacuum oven to remove the absorbed water in the membrane. The prepared composite membranes denoted as PASPMOF$_X$, PASPCOF $_X$ and PASPCM $_X$ (X=0.5 and 0.75%). Similarly, pure SPEEK membrane also synthesised and doped with 85% PA without addition of MOF, COF and CM filler known as PA-SPEEK and the membrane thickness in the range of 80-90µm.The acid doping and uptake level is calculated by the following equations:

$$\text{PA uptake (\%)} = \frac{W_{wet} - W_{dry}}{W_{dry}} \times 100 \quad (1)$$

$$\text{Acid doping level (\%)} = \frac{W_{wet} - W_{dry}/MW_{PA}}{W_{dry}/M_P} \times 100 \quad (2)$$

Here in where W_{wet} and W_{dry} represent membrane weight before and after PA acid doping, respectively, and MW_{PA} and M_P represents as the molecular weights of PA and the repeating unit of the SPEEK, respectively [31].

2.6 Characterizations and measurements

2.6.1 FT-IR, XRD and N_2 adsorption

The prepared material was subjected to chemical functionalities and crystalline property investigations via Fourier-transform infrared spectroscopy and X-Ray Diffraction using a NICOLET, iS50 FT-IR spectrometer and XRD-6100 SHIMADZU X-Ray Diffractometer respectively. The specific surface area was calculated using the BET method (Micromeritics Instrument Corporation model 3Flex), based on data obtained from nitrogen adsorption-desorption experiments at 77K.

2.6.2 Thermal, mechanical and Oxidative stability

The thermal stability of the prepared membrane samples was analyzed using thermo-gravimetric analysis (TGA) with a TG209 instrument from NETZSCH thermal analysis. The testing temperature ranged from 25 to 800 °C at a heating rate of 10 °C/min. Mechanical stability is determined by (TSE502B, WANCE Testing Machine co., LTD). The oxidative stability was determined via submerging the membrane samples into the in Fenton's reagent (3% H_2O_2 solution containing 4 ppm Fe^{2+}) at 80 °C for 24 h [32]. Following this film is taken out from the solution and washed with deionized water to place in a vacuum oven for complete drying. The weight of the dried sample was recorded and weight retention percentage was calculated via the weight difference between before and after Fenton's reagent treated samples.

2.6.3 Proton conductivity

Proton conductivity measurement was carried out via the two-probe AC impedance method. The PA-doped membrane samples are sandwiched between the stainless steel electrodes connected with a heating rod and fix the operating frequency range from 1 Hz to 1 MHz with an amplitude of 10 mV. Following this the proton conductivity is tested at different temperature range from 30 to 130°C under anhydrous conditions without humidification [33].

$$\sigma = \frac{L}{RS} \quad (3)$$

where σ membrane proton conductivity, L, R and S denoted as thickness, resistance and active surface of the membrane samples respectively.

3. Results and discussion

3.1 ^{1}H NMR spectrum of SPEEK

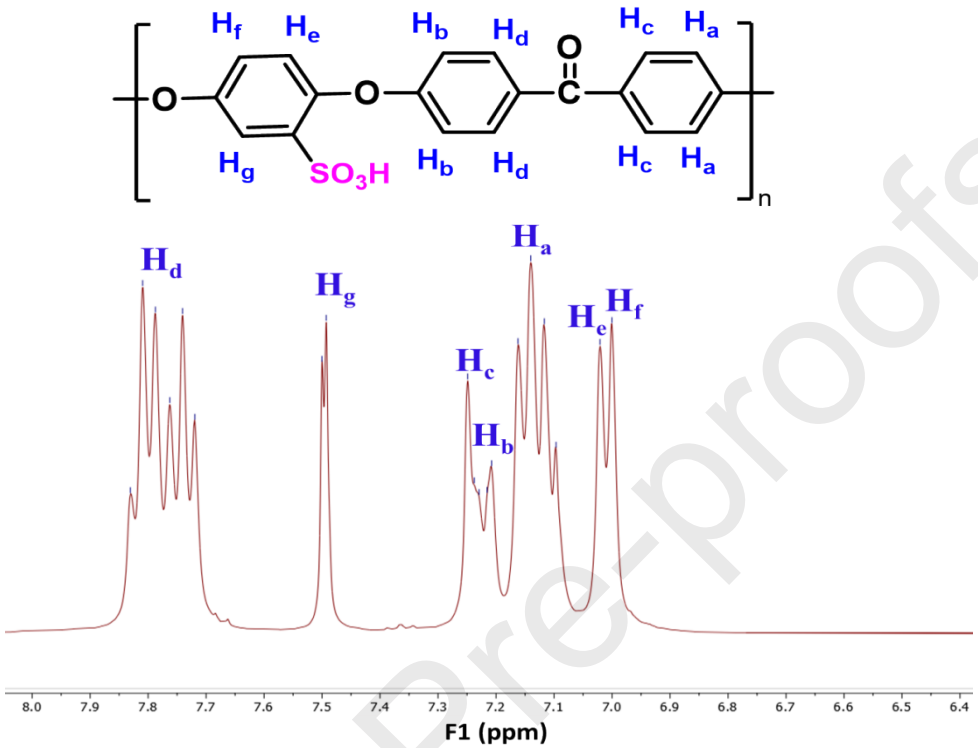

Fig. 2 ^{1}H NMR spectrum of SPEEK

The analysis of SPEEK ^{1}H NMR data is presented in Fig.2, which shows a chemical shift equivalent to the aromatic protons that ranges from 6.0 to 8.0 ppm. Similar to what Naresh et al.[34] found during the sulfonation of PEEK polymer, the resonance peak at 7.5 ppm was attributed to the SO_3H group of SPEEK. The ratio between the Hg signals the singlet at 7.5 ppm, which indicates the SO_3H group content and the integration of other peaks in the SPEEK ^{1}H NMR spectrum can be used to calculate the degree of sulfonation, indicating that the SPEEK polymer was successfully sulfonated [35]. Eq. 4 were used to calculate the degree of sulfonation and it was found to be 0.7.

$$\frac{n}{12-2n} = \frac{S_{Hg}}{S_{H(a,b,c,d,e,f,g)}} \qquad (4)$$

where S_{Hg} is the peak area of the H_g signal, and SH (a, b, c, d, e, f) is the peak area of the signals corresponding to all other aromatic hydrogens. where n is the number of H_g per repeat unit. The degree of sulfonation (DS) is calculated using DS = n ×100%.

3.2 Characterisation of UiO-67 and CM

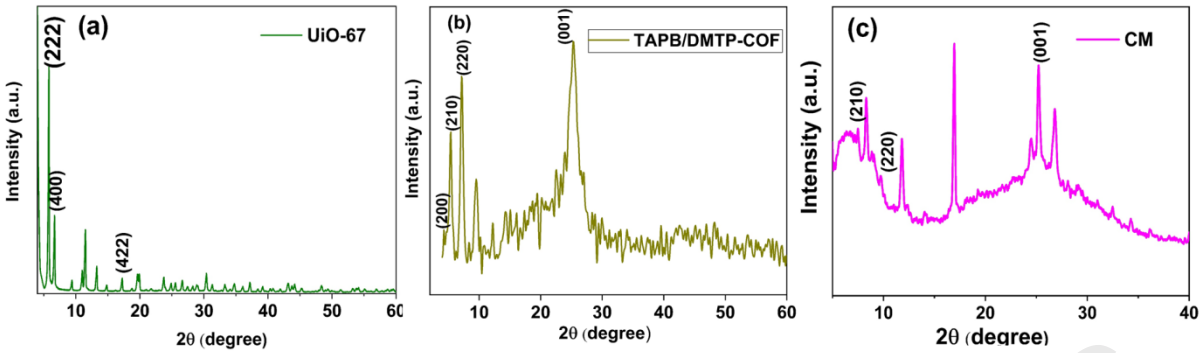

Fig.3 (a-c) XRD pattern of UiO-67, TABP/DMTP COF and CM

For XRD pattern Fig.3 (a) of synthesized UiO-67 at 2θ = 5.6, 6.8, and 17.2° corresponds to the primary characteristic peaks of the (222), (400), and (422) crystal planes well matched with literature report. Fig.3 (b) TAPB-DMTP-COF, exhibit the base peaks at 4.4°, 5.7°, 7.3°, and 25.4° corresponding to (200), (210), (220), and (001) reflection planes indicating the presence of 2D eclipsed stacking TAPB-DMTP− COF in the composite. For Fig.3 (c) CM the base peaks of (222) UiO-67 were suppressed because of CM coating on the MOF surface and additionally, new peaks of pure TAPB-DMTP-COFs conformed and the peaks observed at 7.39° 9.73°, were corresponding to the (210) and (220) plane respectively. Additionally, at 25.28°, a strong diffraction peak corresponding to the (001) plane was observed, which is consistent with the imine-connected 2D polymer sheets 0.35 nm interlayer stacking [36]. These results confirm that the formation of core shell between UiO-67 and TABP-DMTP-COF and its represented as 'CM' [26, 37]. Furthermore, it was also confirmed via FT-IR and the results given in Fig.S2. The Zr-O bonds are associated with the triplet at approximately 769 cm^{-1}, 710 cm^{-1}, and 660 cm^{-1} for UiO-67, representing the longitudinal and transverse modes, respectively. The green-highlighted peaks at 1300–1600 cm^{-1} correspond to the linker's carboxylate stretching (in- and out-of-phase stretching modes of the O-C=O groups [37]. For Fig.S2 COF the peaks 1681 cm^{-1} corresponds to the C=O stretching vibration of DMTP [38] and the formation of imine bonds through condensation between the amino groups of TAPB and the aldehyde groups of DMTP is indicated by the stronger absorption peak of TAPB-DMTP-COF at 1611cm^{-1} [39, 40]. For CM both UiO-67 and COF peaks was observed. These results indicate the TAPB-DMTP COF coated on the UiO-67 surface forms a core shell structure of CM.

3.2.1 N_2 adsorption isotherms and Surface morphology of UiO-67 and CM

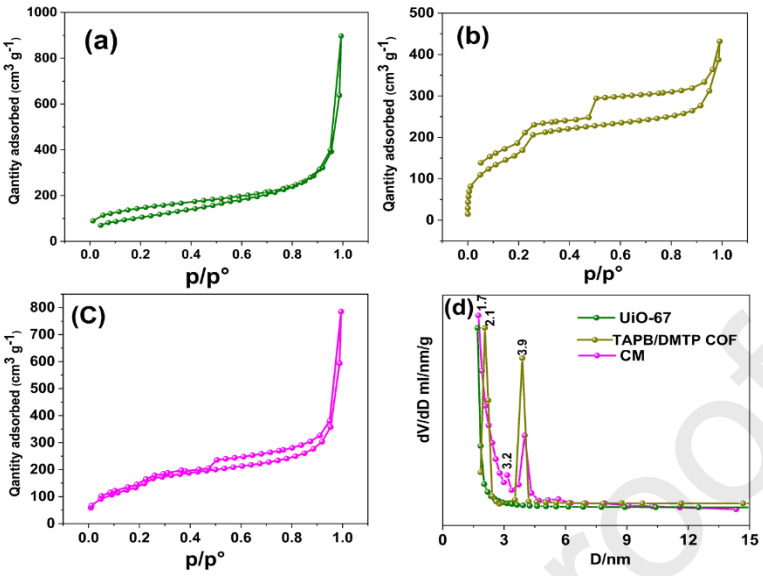

Fig.4 (a-c) N_2 adsorption/desorption isotherms and (d) pore size distribution of UiO-67 TAPB/DMTP COF and CM

The Fig.4 and Table S2 shows the adsorption/desorption curves for pure UiO-67, COF, and CM. In the diagram, UiO-67 demonstrates a typical microporous structure with a pore size center at 1.8 nm. TAPB–DMTP-COFs exhibit a typical mesoporous structure (type IV isotherm) with a pore size center at 2.1 nm and 3.9 nm. As expected, the core–shell MOF@COFs combine the microporous structure of UiO-67 with the mesoporous structure of the TAPB–DMTP COFs. The adsorption-desorption isotherms of CM exhibit the typical characteristics of both micro- (1.7nm) and mesoporosity (3.2nm) (Fig. 4a and b, Table S2). Specific area values obtained using the N2 adsorption isotherms are 1080 m^2/g (UiO-67), 597 m^2/g (COF), and 872 m^2/g (CM). The pore volume values calculated by the BJH method are 0.32 cm^3/g (UiO-67), 0.6 cm^3/g (COF), and 0.04 cm^3/g (CM). The decrease in specific area and pore volume values confirm the growth of the TAPB-TMPTP COF on the UiO-67 surface [19].

Surface morphology and internal distribution investigated via SEM and TEM respectively and the results given in Fig.5 (a-d) [19, 41]. For SEM (Fig.5 (a-b)) Zr- UiO-67 MOF showed well-defined octahedral structure while TAPB/DMTP COF showed spherical morphology structure which is consistent with the literature report [40]. (Fig.5(c-d)) CM showed well dispersed two different morphologies (denoted as a yellow line) combined with a regular polyhedral crystal structure, which is covered with stacked flakes. This particle distribution conforms that TAPB-DMTP COF well coated on the UiO-67. This result confirms the formation of the core-shell structure. Further the with the elemental mapping (Fig.S3) of C, O, and Zr which conforms the formation of core shell structure. This is due to the growth of TAPB-DMTP COF on UiO-67 via Shiff-based condensation reaction [42].

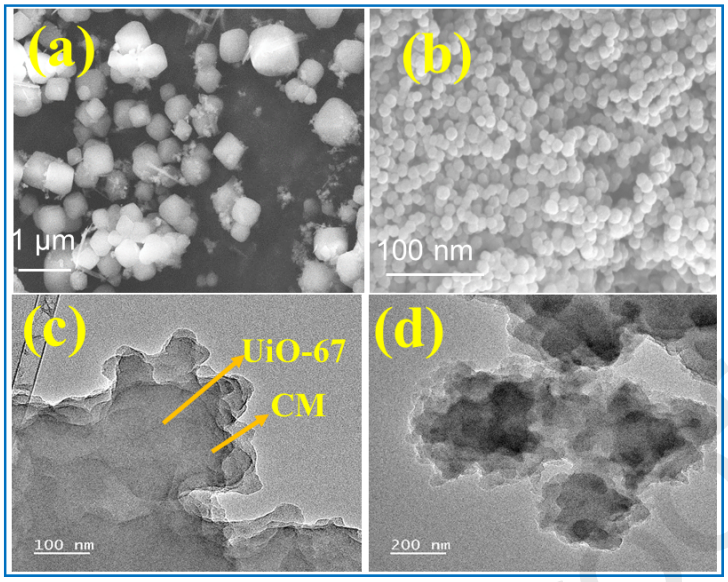

Fig.5 SEM image of (a) UiO-67 and (b) TAPB/DMTP COF (c-d) TEM image of CM core shell MOF (at different scales 100nm and 200nm)

3.3 Membrane characterisations

In Fig. S4, the pristine PA SPEEK membrane shows a broad peak at 22°, indicating a combination of crystalline and amorphous elements. The addition of COF, MOF, and CM additives significantly changed the crystalline properties of the membranes. Fig. S4 (a), the PASPMOF membrane exhibited a new crystalline peak at 17.2°, corresponding to the (422) plane, confirming the presence of UiO-67. On the other hand, the PASPCOF membranes base peak became broadened, and no additional peak was observed. This is attributed to the higher uptake of PA, leading to increased membrane swelling and affecting the polymer's crystallinity. In contrast, both PASPCM-0.5 and PASPCM-0.75 membranes showed a high-intensity XRD with a high crystalline base peak at 22° compared to the pristine COF and MOF membranes. This enhancement is due to the heterogeneous (meso/micro) structure of CM, which increases the acid-base interaction between SPEEK and CM and FT-IR confirmed it. FT-IR spectra of prepared membrane results given in Fig.S4 (a, b and c). all the membranes showed similar sharp peaks observed at 1077 cm^{-1} ,1254 cm^{-1}, 1490 cm^{-1},1472 cm^{-1} corresponds to the conforms the presence of sulfonic acid group (asymmetric O=S=O stretching, symmetric O=S=O stretching, and S=O stretching respectively) in SPEEK matrix [43] and broad peak appeared at 2500-3500 cm^{-1} which corresponds to the mixture of N–H and C–H in the range of 2250–3180 cm^{-1} (Fig.S4(a)). This was accompanied by the emergence of an OH broad peak in the range of 3270–3550 cm^{-1} caused by the formation of an H-bonding network between the SPEEK/CM and Phosphoric acid [44]. overall results reveal that the added CM well intercalates into the SPEEK matrix, and this results in good agreement with SEM results given in Fig.S5 (a-b). PASPEEK (Fig.S5 (a)) showed a smoother surface, while (b) PASPMOF-0.75 membranes showed a rougher surface with pinhole, and the UiO-67 particles were non-uniformly (particle agglomeration) distributed on the SPEEK surface. This is due to the rigid and brittleness of UiO-67, making the membrane surface uneven. In contrast (c) PASPCOF-0.75, COF particles (sphered morphology) are well dispersed on the SPEEK surface because

of its acid base formation of COF with SPEEK enhance the dispersing ability of COF. Similarly, PASPCM-0.75 (Fig.S5 (d)) showed rougher and CM particles are finely dispersed on the PASPEEK surface.

3.4 Acid uptake and swelling ratio

The PA doping process of PASPEEK, PASPMOF-0.5, PASPMOF-0.75, PASPCOF-0.5, PASPCOF-0.75, PASPCM -0.5, and PASPCM -0.75 membranes is depicted in Fig.S6 (a) and Table S3, along with the relative swelling in area and thickness. Thickness-directed swelling is typically substantially greater than length- and width-directed swelling for polymer membranes submerged in the small molecule-containing solution. There are two potential causes for this (1) The solution casting method produces a membrane that is more prone to chain entanglement in both the width and length directions because the molecules tend to lay flat on the glass plate during the drying process due to gravity; (2) The swelling in the thickness direction will further increase due to fewer molecular chain entanglements because of the significant dimension differences between the thickness and length/width of the thin membrane (at least two orders of magnitude) [45]. According to the table value all the membranes swelling ratio increased via a thickness direction which is much higher than the area swelling. Additionally, as the chain length increases, the in-plane chain entanglement is strengthened, which causes the thickness swelling of the membrane samples to rise continuously. The acid doping level, area, and thickness of the membrane increased in the order of PASPMOF-0.5<PASPMOF-0.75<PASPEEK<PASPCOF-0.5, PASPCOF-0.75<PASCM-0.5< m-PBI PASCM-0.75. For SPEEK, MOF loaded membrane showed the lowest and controlled PA uptake. This is due to the absence of active functional groups (amino groups) to attract PA and the bulkiness of MOF may restrict the polymer chain mobility in SPEEK [46]. In contrast, COF membranes showed an increased PA absorption trend. This is due to the presence of excess amino functionalities in TABP/DMTP COF, creating a hydrogen bonding with PA molecules (P=O---H–N bond) to allow more PA uptake[47]. However, higher PA uptake affects the membrane stability and increases the swelling character. On the other hand, CM incorporated membrane showed high PA uptake with good film-formed membranes (Given in Fig.S1). This is due to the heterogeneous combination of UiO-67 and COF providing controlled as well increased PA uptake. Further The more doped PA molecules would generate an increased dynamic hydrogen bonding network for proton transport, thus achieving a high conductivity. specifically, For PASCM-0.75 hybrid membranes showed high thickness value and area swelling than PBI.

3.5 Acid doping

For anhydrous conductivity PA doping level plays a vital role, especially in PBI polymer presence of basic functionalities creates strong hydrogen bonded with PA molecules. Further PA doping level chiefly controls the proton conductivity in PEM [48]. Protons mostly transfer between phosphate anions and protonated benzimidazole rings when PA doping levels are low (typically below 2). This is because PA molecules in the membranes are immobilized on the fundamental units of polymers. As the doping level increases, the mixed H_2PO_4 undergoes successive proton transfer and anion reorientation, which contribute to the proton migration of both bounded and free PA molecules. Here the prepared membrane showed the acid doping level from 0.45 % to 0.82 % which is lower than PBI (4.8%). Fig.S6 (a) and Table S3 showed the Acid doping uptake level of prepared membranes. It can be seen that the doping level gradually increased upon the CM addition this is due to strong hydrogen bond formation between base functionalities present in the core shell structure absorbs more phosphoric acids.

However, it does not affect the membrane stability and it was confirmed by the tensile results given in Fig.S9 (b).

3.7 Proton conductivity

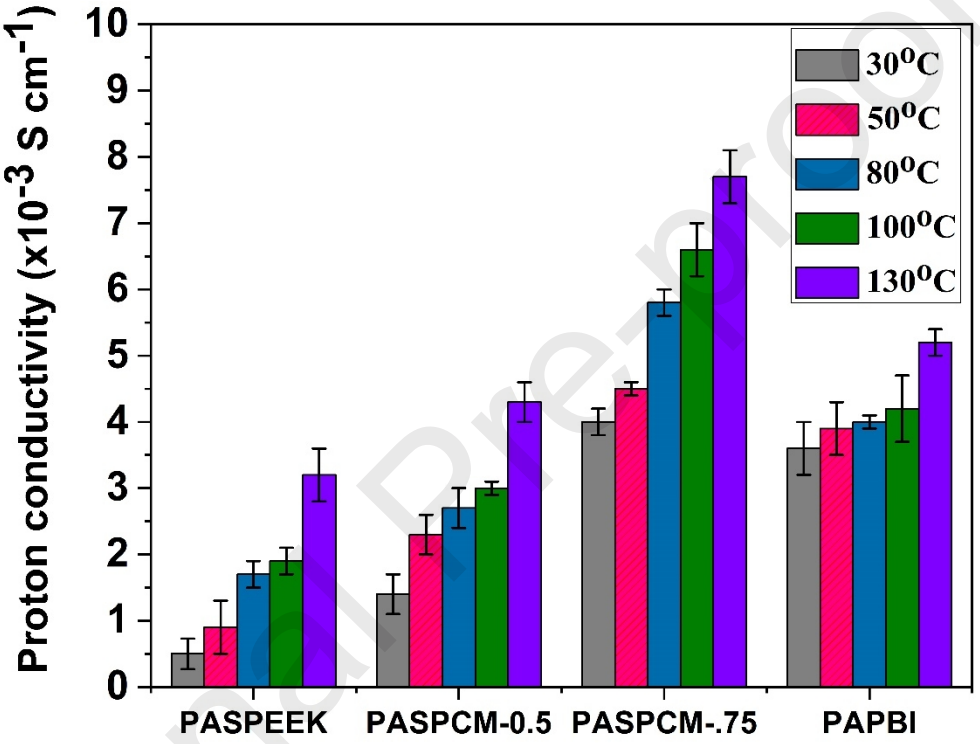

Fig. 6 Proton conductivity value of PASPEEK, PASPCM-0.5, PASPCM-0.75 and PA PBI membranes at different temperature range from 30°C to 130 °C.

Using the AC impedance technique, PASPEEK, PASPMOF, PASPCOF and PASPCM membrane resistance was measured; the results are shown in **Fig. S7 and S8.** This figure also includes a Nyquist plot of the extended and complete graph resistance values under various temperature conditions (30 to 130 °C) based on the resistance values proton conductivity was mathematically calculated using **Eq.3 (Refer section 2.6.3)** and the results displayed in Table **S4 and Fig.6**. It is evident in all the membrane samples that the membrane resistance value gradually decreased when increasing the temperature from 30 °C to 130 °C which implies the high ionic conducting properties of the membranes. Because resistance is inversely proposal to ionic conductivity. From **Fig.6,** and **Table S4** results the conductivity increases in the order of PASPMOF-0.75<PASPMOF-0.5<PASPEEK<PASPCOF-0.5<PASCOF-0.75<PASPCM-0.5<PAPBI<PASPCM-0.75. In the case of commercial PBI, we discovered that at a doping level of 4.5, the conductivity reached 5×10^{-3} Scm^{-1}, which is in good accordance with literature reports [49]. In general, PA-doped PBI demonstrated poor conductivity example in the absence of humidification. Bouchet and Siebert et al. [50] reported an anhydrous conductivity of 7×10^{-6}

S cm^{-1} at a temperature of 30 °C and an H_3PO_4 doping level of 3.05. Fontanella et al. [51] reported dry PBI membrane conductivity is 4.5 × 10^{-5} Scm^{-1} at high doping level (DL = 6 at room temperature).For Uio-67 contained membrane showed the lowest conductivity, 6 ×10^{-4} S cm^{-1}, and increased filler content reduced the proton conductivity. This is due to the following reasons such as the lack of active functional groups(-NH/NH_2) , rigid and stable structure of UiO-67 hindering the proton mobility and low PA uptake[52, 53]. While COF-incorporated SPEEK exhibits high conductivity (3.5×10^{-3} S cm^{-1}), this is due to the presence of –NH increasing the PA affinity by creating an acid-base formation between SPEEK/COF with H_3PO_4. Similarly, CM incorporated membranes showed increased proton conductivity value up to 7.6 × 10^{-3} Scm^{-1} at 130 °C. Increasing proton conductivity is influenced by two factors (i) intermolecular hydrogen bonding between polymer and imine group of coreshell filler creates an acid-base pair (ii) Numerous hydrogen bonds with H_3PO_4 were formed as a result of the abundant -NH group in COF interacting with the P O---H-N bond [7]. Further, the mesoporous and microporous heterogeneous porous structures act as proton carriers to increase the proton mobility of the membranes [19]. A heterogeneous micro-/mesoporous channel is created by combining two different types of pores across the UiO-67@TAPB-DMTP-COF core-shell interface. By forming more heterogeneous micro- and mesopores, it is possible to rationally design proton-conductive porous materials. The synergy between the various components of the UiO-67@TAPB-DMTP-COF composites is crucial for enhancing proton conduction. The advantages of MOF@COF hybridization are numerous. Firstly, the membrane's chemical stability and proton carrier transfer ability can be improved, resulting in better proton carrier loading and easier hydrogen bond reorganization. This enhancement is due to the synergistic interaction between the various components of MOFs and COFs, which collectively optimize the heterogeneous channels [19]. Based on the above results suggest that the prepared PASPCM-0.75 membrane is considered a potential PEM for HT-PEMFC applications.

3.6 Tensile strength, Oxidative and thermal stability

The commercial PBI exhibited a low tensile value of approximately 11.8MPa, whereas PASPCM-0.75 demonstrated a significantly higher tensile value of 27.3MPa, marking a 131.1% increase compared to PA PBI. This substantial increase in tensile strength renders PASPCM-0.75 more suitable for fuel operation, given the high PA doping and exceptional mechanical stability within hybrid PEM structures. Notably, these values surpass those of other MOF-based PEMs documented in the literature (see **Table S5**). [54]. These encouraging findings validate the enhanced membrane durability attributed to hybrid PEMs, particularly due to their elevated mechanical stability. Furthermore, they position hybrid PEMs as viable alternatives to commercial PA PBI.

Fig.S9 (b-c) showed the oxidative stability of the prepared membrane and all the membranes were subject to a strong oxidizing environment for 15 days and heated at 100 °C. We measure the membrane weight before and after immersing Fenton's reagent (Digital photograph of Fenton's reagent with membrane sample image given in Fig.S9(c)). In the beginning, the sample weight of all membranes increased, especially the pristine PASPEEK showed higher weight % but after heating the PASPEEK got harder and brittle which is attributed to the greater absorption of solution-induced polymer degradation. As a result, PASPEEK membrane loses it membrane stability it breaks down into small pieces. Whereas PASPCM-0.5 and PASPCM-0.75 membrane slight weight loss was observed and the membrane had a weight retention % of 92.3 to 94.9% respectively. For commercial PA PBI partial weight loss was observed and the oxidative stability reached up to 90%, which is lower

than PASPCM-0.75 membranes. This improved oxidative stability is attributed to the chemical robustness (because of pi–pi conjugated structures) of Core TABP-DMTP COF and strong acid-base formation between PA/SPEEK and CM to prevent the membrane from free radical attack.

To assess the hybrid membranes' thermal properties, TGA analyses were carried out. The TGA curves for pure PA/SPEEK and PASPCM hybrid membranes in a nitrogen environment are displayed in Fig.S9 (d). Three separate phases of weight loss are seen. The first weight loss occurs in the temperature range of 100 to 120 °C and is caused by thermal dehydration, which is the removal of physically attached water (residual humidity). The primary cause of the second weight loss in the 300–400 °C range is the thermal breakdown of the sulfonic acid groups in SPEEK. The third zone of weight loss, which is between 450°C and 800 °C, is corresponds to the polymer backbone. These findings show that all of the membranes have enough thermal stability to be used as proton conducting materials up to 300 °C [55]. While the TGA profiles of each membrane are similar and indicate the start of thermal degradation, the mass loss slope varies. The blend membranes' onset temperatures are comparatively higher than those of the SPEEK membrane. Furthermore, at 500 °C PASPCM-0.5 and PASPCM-0.75 showed extended thermal weight loss of 33% and 30% than PA/SPEEK 40%. This increased thermal degradation temperature clearly revealed that the added CM additive increase the membranes thermal stability. This is due to the excellent chemical stability of TABP-DMTB COF and the strong hydrogen bonding network increases the membrane thermal stability. According to Xu et al. [56], the stability of a two-dimensional (2D) COF is influenced by two factors: the interlayer force and the bonding strength between the components of the 2D layers. The layered stacking structure is primarily directed by the interlayer interactions, which have a major impact on the crystallinity and porosity of the resulting COFs. Imine-linked COFs exhibit a partial positive charge for the carbon and a negative charge for the nitrogen due to the polarization of the C=N bond. Each of the 12 polarized C=N segments that make up a macrocycle in a hexagonal 2D COF destabilizes the layered structure due to electrostatic repulsion, as predicted theoretically.

4. Conclusion

To enhance the mechanical stability and anhydrous proton conductivity of PEM, in this work novel phosphoric acid-doped SPEEK-based hybrid membranes were synthesized. The degree of sulfonation, confirmed by ^{1}H NMR to be 70%. Surface area and pore size distribution of MOF, COF and the core-shell structure were confirmed by BET and are critical factors contributing to the improved properties of the membranes. SPEEK with different additives and its performance systematically studied. (i) MOF-incorporated SPEEK showed low PA uptake, good dimensional stability, low proton conductivity, and good mechanical stability. (ii) COF-incorporated SPEEK showed higher PA uptake than MOF. Higher PA absorption causes serious membrane swelling, leading to poor mechanical stability; however, pi-pi conjugated structure provides good chemical stability. (iii) core-shell structure greatly alters the SPEEK membrane properties than individual COF and MOF. The blending of CM into SPEEK, which enhances thermal stability above 300 °C and mechanical stability even at high PA loading, is particularly noteworthy. The highest anhydrous conductivity achieved was 7.6×10^{-3} S cm^{-1} at 130 °C, with mechanical stability of 27.3 MPa. These values represent increases of 68.9% and 131.36%, respectively, compared to commercial PA PBI membranes. These results suggest that the prepared membranes overcome the practical limitation of PA PBI membranes and exhibit increased stability even at higher ADL than PA PBI membranes. This is due strong acid-base interaction between SPEEK and CM, which facilitates increased PA doping and thus

higher proton conductivity, along with the superior chemical and oxidative stability properties of CM that provide enhanced membrane stability and protection against free radical attack, are key findings of this work. PASPCM-0.75 membranes show excellent mechanical stability and proton conductivity than commercial PA PBI membranes. which makes them a good alternate for high-temperature PEM fuel cell (HT-PEMFC) applications.

Acknowledgments

This work was supported by National Key R&D Program of China (2018YFE0121200), National Natural Science Foundation of China (22308129), and Jiangsu Province Excellent Postdoctoral Program (2023ZB864), the Priority Academic Program Development (PAPD) of Jiangsu Higher Education Institutions.

References

[1] X. Zhao, L. Wang, Y. Zhou, B. Pan, R. Wang, L. Wang, X. Yan, Energy management strategies for fuel cell hybrid electric vehicles: Classification, comparison, and outlook, Energy Convers. Manage. , 270 (2022) 116179.

[2] X. Zhao, Y. Zhou, L. Wang, B. Pan, R. Wang, L. Wang, Classification, summarization and perspective on modeling techniques for polymer electrolyte membrane fuel cell, Int. J. Hydrogen Energy, 48 (2023) 21864-21885.

[3] S.-I. Kim, S.-y. Lim, M. Son, T. Kim, Highly Active and Stable Bimetallic Ordered Catalysts for Oxygen Reduction Reaction Improvement in Polymer Exchange Membrane Fuel Cells, Appl. Surf. Sci., 656 (2024) 159620.

[4] X. Chen, Y. Zhang, S. Xu, F. Dong, Bibliometric analysis for research trends and hotspots in heat and mass transfer and its management of proton exchange membrane fuel cells, Appl. Energy 333 (2023) 120611.

[5] H.K. Jia, J.H. Yan, B.F. Yin, Z.L. Chen, W. Wei, S.P. Chen, Studies on heat transfer performance of miniature cross-flow heat exchangers with perforated fins for direct methanol fuel cells, Appl. Therm. Eng. , 243 (2024) 122559.

[6] W. Zhang, Z. Jiang, Y. Lu, Z. He, Z. Shao, J. Yu, Optimization of porous layer structure of high-temperature proton exchange membrane fuel cell based on deep learning and Monte Carlo method, Int. J. Hydrogen Energy, 50 (2024) 1004-1019.

[7] K. Divya, M.R. Asghar, N. Bhuvanendran, H. Liu, W. Zhang, Q. Xu, S.Y. Lee, H. Su, Influence of incorporation of Zeolitic Imidazolate Framework-67 on the performance and stability of sulfonated Polyvinylidene fluoride proton exchange membrane for fuel cell applications, React. Funct. Polym. , 199 (2024) 105903.

[8] C. Li, X. Xu, H. Hu, N. Mei, Y. Yang, Numerical Investigation Into the Effect of Structural Parameters of Parallel Flow Field With Cooling Channels on Fuel Cell Performance, J. Electrochem. En. Conv. Stor., 19 (2021) 010903.

[9] F. Wang, S. Deng, H. Zhang, J. Wang, J. Zhao, H. Miao, J. Yuan, J. Yan, A comprehensive review on high-temperature fuel cells with carbon capture, Appl. Energy 275 (2020) 115342.

[10] J. Baek, H. Son, S.W. Joo, M. Kim, G. Lee, Bimetallic zeolitic imidazole framework-derived sulfur-doped porous carbon as highly efficient catalysts for oxygen reduction reaction in proton exchange membrane fuel cells, Appl. Surf. Sci., 642 (2024) 158609.

[11] X. Baozhong, O. Savadogo, The effect of acid doping on the conductivity of polybenzimidazole (PBI), J. New Mater. Electrochem. Syst. , 2 (1999) 95-101.

[12] L.K. Seng, M.S. Masdar, L.K. Shyuan, Ionic Liquid in Phosphoric Acid-Doped Polybenzimidazole (PA-PBI) as Electrolyte Membranes for PEM Fuel Cells: A Review, Membranes, 11 (2021) 728.

[13] L. Hong, B. Wang, C. Zhao, Phosphoric acid doped high temperature proton exchange membranes based on comb-shaped polymers with quaternized graft architectures, Appl. Surf. Sci., 483 (2019) 785-792.

[14] J. Zhao, D. Song, J. Jia, N. Wang, K. Liu, T. Zuo, Q. Che, Constructing proton exchange membranes with high and stable proton conductivity at subzero temperature through vacuum assisted flocculation technique, Appl. Surf. Sci., 585 (2022) 152579.

[15] Z. Li, Y. Zhou, J. Hu, C. Shi, S. Liu, Y. Ge, T. Zhou, Y. Ye, Incorporating flexible sulfonate-imidazolium ion pair-functionalized MOF in cross-linked polyvinyl alcohol membrane for achieving superprotonic conduction, Chem. Eng. J. , 480 (2024) 148146.

[16] Y. Devrim, C.O. Colpan, Assessment of polybenzimidazole/MOF composite membranes for the improvement of high-temperature PEM fuel cell performance, Int. J. Hydrogen Energy, 58 (2024) 470-478.

[17] M.-Y. Zhang, X.-N. Qin, C.-X. Zhang, Q.-L. Wang, Chlorosulfonated Polyphenylene Ether Metal–Organic Framework Nanomaterial Composite Proton Exchange Membranes for Fuel Cells, ACS Appl. Nano Mater. , 7 (2024) 7063-7071.

[18] H.R. Abuzeid, A.F.M. El-Mahdy, S.-W. Kuo, Covalent organic frameworks: Design principles, synthetic strategies, and diverse applications, Giant, 6 (2021) 100054.

[19] S. Liu, H. Li, Y. Shuai, Z. Ding, Y. Liu, Imidazole encapsulated in core–shell MOF@COFs with a high anhydrous proton conductivity, Materials Advances, 3 (2022) 8647-8655.

[20] M. Furtmair, J. Timm, R. Marschall, Sulfonation of porous materials and their proton conductivity, Microporous Mesoporous Mater. , 312 (2021) 110745.

[21] X. Wang, Y. Rong, F. Wang, C. Zhang, Q. Wang, High performance proton exchange membranes with double proton conduction pathways by introducing MOF impregnated with protic ionic liquid into SPEEK, Microporous Mesoporous Mater. , 346 (2022) 112314.

[22] C. Guo, F. Duan, S. Zhang, L. He, M. Wang, J. Chen, J. Zhang, Q. Jia, Z. Zhang, M. Du, Heterostructured hybrids of metal–organic frameworks (MOFs) and covalent–organic frameworks (COFs), J. Mater. Chem. A 10 (2022) 475-507.

[23] S. Hao, Z. Jia, Covalent organic frameworks membranes: Fabrication and applications, Microporous Mesoporous Mater. , 361 (2023) 112742.

[24] H. Xu, S. Tao, D. Jiang, Proton conduction in crystalline and porous covalent organic frameworks, Nat. Mater. , 15 (2016) 722-726.

[25] S. Tao, L. Zhai, A.D. Dinga Wonanke, M.A. Addicoat, Q. Jiang, D. Jiang, Confining H3PO4 network in covalent organic frameworks enables proton super flow, Nat. Commun. , 11 (2020) 1981.

[26] Y. Xie, T. Zhang, Y. Chen, Y. Wang, L. Wang, Fabrication of core-shell magnetic covalent organic frameworks composites and their application for highly sensitive detection of luteolin, Talanta, 213 (2020) 120843.

[27] X. Zhao, K. Sasaki, Advanced Pt-Based Core–Shell Electrocatalysts for Fuel Cell Cathodes, Acc. Chem. Res., 55 (2022) 1226-1236.

[28] P. Salarizadeh, M. Javanbakht, M.B. Askari, K. Hooshyari, M. Moradi, H. Beydaghi, M. Rastgoo-Deylami, M. Enhessari, Novel proton conducting core–shell PAMPS-PVBS@Fe2TiO5 nanoparticles as a reinforcement for SPEEK based membranes, Sci. Rep., 11 (2021) 4926.

[29] K. Divya, H. Liu, W. Zhang, Q. Xu, H. Su, Sulfonated poly (ether ether ketone)/MOF hybrid polymer electrolyte membrane with ultra-low methanol permeability for enhanced direct methanol fuel cell performance, J. Appl. Polym. Sci. , 141 (2024) e55749.

[30] K. Divya, D. Rana, M.S. Sri Abirami Saraswathi, A. Nagendran, Sulfonated poly (ether sulfone) composite membranes customized with polydopamine coated molybdenum disulfide nanosheets for renewable energy devices, Polymer, 175 (2019) 255-264.

[31] J. Wu, F. Wang, X. Fan, J. Chu, F. Cheng, F. Hu, H. Liu, Q. Zhang, Z. Xu, C. Gong, Phosphoric acid-doped Gemini quaternary ammonium-grafted SPEEK membranes with superhigh proton conductivity and mechanical strength for direct methanol fuel cells, J. Membr. Sci., 672 (2023) 121431.

[32] N. Zhang, B. Wang, Y. Zhang, F. Bu, Y. Cui, X. Li, C. Zhao, H. Na, Mechanically reinforced phosphoric acid doped quaternized poly(ether ether ketone) membranes via cross-linking with functionalized graphene oxide, Chem. Commun. , 50 (2014) 15381-15384.

[33] S. Bano, Y.S. Negi, K. Ramya, Studies on new highly phosphonated poly (ether ether ketone) based promising proton conducting membranes for high temperature fuel cell, Int. J. Hydrogen Energy, 44 (2019) 28968-28983.

[34] R. Naresh Muthu, S. Rajashabala, R. Kannan, Synthesis and characterization of polymer (sulfonated poly-ether-ether-ketone) based nanocomposite (h-boron nitride) membrane for hydrogen storage, Int. J. Hydrogen Energy, 40 (2015) 1836-1845.

[35] P. Xing, G.P. Robertson, M.D. Guiver, S.D. Mikhailenko, K. Wang, S. Kaliaguine, Synthesis and characterization of sulfonated poly(ether ether ketone) for proton exchange membranes, J. Membr. Sci., 229 (2004) 95-106.

[36] B.J. Smith, A.C. Overholts, N. Hwang, W.R. Dichtel, Insight into the crystallization of amorphous imine-linked polymer networks to 2D covalent organic frameworks, Chem. Commun. , 52 (2016) 3690-3693.

[37] E. Binaeian, Y. Li, H.-A. Tayebi, D. Yuan, Enhancing toxic gas uptake performance of Zr-based MOF through uncoordinated carboxylate and copper insertion; ammonia adsorption, J. Hazard. Mater. , 416 (2021) 125933.

[38] L. Yu, J. Zhang, J. Li, L. Sun, Q. Zhang, B. Yang, M. Huang, B. Xu, Rapid, simple, and simultaneous electrochemical determination of cadmium, copper, and lead in Baijiu using a novel covalent organic framework based nanocomposite, Front. Chem. , 12 (2024) 1374898.

[39] Y. Peng, X. Zhang, Y. Zhang, C. Zhou, X. Wu, M. Li, Y. Hua, Stability and adsorption performance of UiO-67 for uranium(VI) in solution, J. Radioanal. Nucl. Chem. , 333 (2024) 305-315.

[40] T. Zhang, C. Gao, W. Huang, Y. Chen, Y. Wang, J. Wang, Covalent organic framework as a novel electrochemical platform for highly sensitive and stable detection of lead, Talanta, 188 (2018) 578-583.

[41] C.G. Piscopo, F. Trapani, A. Polyzoidis, M. Schwarzer, A. Pace, S. Loebbecke, Positive effect of the fluorine moiety on the oxygen storage capacity of UiO-66 metal–organic frameworks, New J. Chem. , 40 (2016) 8220-8224.

[42] Y. Li, M. Karimi, Y.-N. Gong, N. Dai, V. Safarifard, H.-L. Jiang, Integration of metal-organic frameworks and covalent organic frameworks: Design, synthesis, and applications, Matter, 4 (2021) 2230-2265.

[43] S. Qu, M. Li, C. Zhang, Y. Sun, J. Duan, W. Wang, J. Li, X. Li, Sulfonated Poly(ether ether ketone) Doped with Ammonium Ionic Liquids and Nano-Silicon Dioxide for Polymer Electrolyte Membranes, Polymers, 11 (2019) 7.

[44] P. Sithambaranathan, M.M. Nasef, A. Ahmad, A. Abbasi, T.M. Ting, Composite Proton-Conducting Membrane with Enhanced Phosphoric Acid Doping of Basic Films Radiochemically Grafted with Binary Vinyl Heterocyclic Monomer Mixtures, Membranes, 13 (2023) 105.

[45] G. Liu, A. Wang, W. Ji, L. Zhang, J. Wu, T. Zhang, H. Tang, H. Zhang, Soluble ultra-high molecular weight poly(4,4′-diphenylether-5,5′-bibenzimidazole) based membranes with remarkable mechanical strength and specific proton conductivity for high temperature proton exchange membrane fuel cells, J. Membr. Sci., 693 (2024) 122348.

[46] J. Chen, L. Wang, L. Wang, Highly Conductive Polybenzimidazole Membranes at Low Phosphoric Acid Uptake with Excellent Fuel Cell Performances by Constructing Long-Range Continuous Proton Transport Channels Using a Metal–Organic Framework (UIO-66), ACS Appl. Mater. Interfaces 12 (2020) 41350-41358.

[47] V. Joseph, A. Nagai, Recent advancements of covalent organic frameworks (COFs) as proton conductors under anhydrous conditions for fuel cell applications, RSC Adv. , 13 (2023) 30401-30419.

[48] J. Wu, S. Nie, H. Liu, C. Gong, Q. Zhang, Z. Xu, G. Liao, Design and development of nucleobase modified sulfonated poly(ether ether ketone) membranes for high-performance direct methanol fuel cells, J. Mater. Chem. A 10 (2022) 19914-19924.

[49] L. Qingfeng, H.A. Hjuler, N.J. Bjerrum, Phosphoric acid doped polybenzimidazole membranes: Physiochemical characterization and fuel cell applications, J. Appl. Electrochem., 31 (2001) 773-779.

[50] R. Bouchet, E. Siebert, Proton conduction in acid doped polybenzimidazole, Solid State Ionics, 118 (1999) 287-299.

[51] J.J. Fontanella, M.C. Wintersgill, J.S. Wainright, R.F. Savinell, M. Litt, High pressure electrical conductivity studies of acid doped polybenzimidazole, Electrochim. Acta, 43 (1998) 1289-1294.

[52] D. Huang, L. Wu, Q. Kang, Z. Shen, Q. Huang, W. Lin, F. Pei, Y. Huang, Amino-modified UiO-66-NH2 reinforced polyurethane based polymer electrolytes for high-voltage solid-state lithium metal batteries, Nano Res. , (2024).

[53] H.T. Lai, N.Q.M. Tran, L.H.T. Nguyen, T.B.N. Le, C.C. Nguyen, A.T.T. Pham, T.L.H. Doan, S. Park, J. Hong, G.J. Snyder, T.B. Phan, Low experimental thermal conductivity of zirconium metal-organic framework UiO-66, Appl. Phys. Lett. , 124 (2024) 152205.

[54] Z. Yue, Y.-B. Cai, S. Xu, Phosphoric acid-doped cross-linked sulfonated poly(imide-benzimidazole) for proton exchange membrane fuel cell applications, J. Membr. Sci., 501 (2016) 220-227.

[55] S.G. Peera, S. Meenakshi, K.H. Gopi, S.D. Bhat, P. Sridhar, S. Pitchumani, Impact on the ionic channels of sulfonated poly(ether ether ketone) due to the incorporation of polyphosphazene: a case study in direct methanol fuel cells, RSC Adv. , 3 (2013) 14048-14056.

[56] H. Xu, J. Gao, D. Jiang, Stable, crystalline, porous, covalent organic frameworks as a platform for chiral organocatalysts, Nat. Chem. , 7 (2015) 905-912.

Graphical abstract

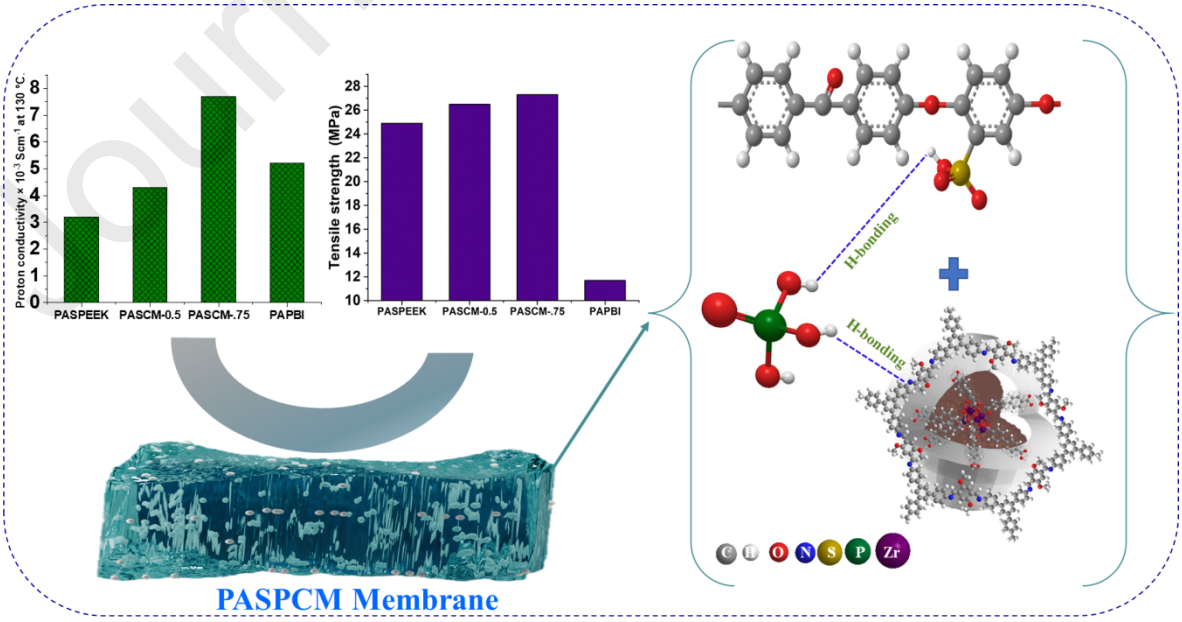

667

668 **Highlights**

669 Degree of sulfonation of poly (ether ether ketone) (SPEEK) is found to be 70%.

670 A novel phosphoric acid doped core shell hybrid PEM was developed via solution casting
671 method

672 Core shell @ CM enhances anhydrous proton conductivity, reducing PA loss.

673 High mechanical stability than commercial PA PBI

674 Exceptional chemical and thermal durability for potential long-term stability.

675

676